SAND2007-8155C

Compact, narrow-linewidth, tunable ultraviolet laser source for detecting Hg emissions

Alexandra A. Hoops*[a], Roger L. Farrow[a], Paul Schulz[a], Thomas A. Reichardt[a], Ray P. Bambha[a], Randal L. Schmitt[b], and Dahv A. V. Kliner[a]
[a]Sandia National Laboratories, PO Box 969 MS 9056, Livermore, CA USA 94551
[b]Sandia National Laboratories, PO Box 5800 MS 1423, Albuquerque, NM USA 87185

ABSTRACT

Recent EPA regulations targeting mercury (Hg) emissions from utility coal boilers have prompted increased activity in the development of reliable chemical sensors for monitoring Hg emissions with high sensitivity, high specificity, and fast time response. We are developing a portable, laser-based instrument for real-time, stand-off detection of Hg emissions that involves exciting the Hg ($6\,^3P_1 \leftarrow 6\,^1S_0$) transition at 253.7 nm and detecting the resulting resonant emission from Hg ($6\,^3P_1$). The laser for this approach must be tunable over the Hg absorption line at 253.7 nm, while system performance modeling has indicated a desired output pulse energy ≥0.1 μJ and linewidth ≤5 GHz (full width at half-maximum, FWHM). In addition, the laser must have the requisite physical characteristics for use in coal-fired power plants. To meet these criteria, we are pursing a multistage frequency-conversion scheme involving an optical parametric amplifier (OPA). The OPA is pumped by the frequency-doubled output of a passively Q-switched, monolithic Nd:YAG micro-laser operating at 10-Hz repetition rate and is seeded by a 761-nm, cw distributed-feedback diode laser. The resultant pulse-amplified seed beam is frequency tripled in two nonlinear frequency-conversion steps to generate 253.7-nm light. The laser system is mounted on a 45.7 cm × 30.5 cm breadboard and can be further condensed using custom optical mounts. Based on simulations of the nonlinear frequency-conversion processes and current results, we expect this laser architecture to exceed the desired pulse energy. Moreover, this approach provides a compact, all-solid-state source of tunable, narrow-linewidth visible and ultraviolet radiation, which is required for many chemical sensing applications.

Keywords: harmonic generation and mixing, optical parametric amplifier, mercury monitoring

1. INTRODUCTION

Monitoring of mercury emissions from coal-fired power plants requires a reliable chemical sensor that can operate with high sensitivity, high specificity, and a fast time response. Current continuous emissions monitors for mercury implement extractive techniques: a sample of the flue gas is removed with a probe and transferred from the stack to the point of analysis. Multiple problems associated with the probe and sampling lines, including plugging of the probe and chemical reactions within the sampling lines, degrade the measurement capabilities of these methods. In contrast, optical techniques are unique in their ability to analyze the flue gas *in situ*, thereby avoiding the difficulties associated with sample extraction and conditioning. To meet the need for a real-time, non-invasive method for monitoring mercury emissions, we are developing laser-based techniques for short-range, sensitive detection of the two primary forms of vapor-phase mercury emitted by utility coal boilers: elemental mercury, Hg^0, and mercuric chloride, $HgCl_2$. We have previously demonstrated the ability to detect $HgCl_2$ using a nonlinear frequency-converted fiber-based laser source,[1] and the current work examines the design and performance of a laser for detecting Hg^0.

The detection approach for Hg^0 involves exciting the Hg ($6\,^3P_1 \leftarrow 6\,^1S_0$) transition at 253.7 nm and detecting the resulting resonant emission from Hg ($6\,^3P_1$). Consequently, the laser source must be tunable over the Hg^0 absorption line at 253.7 nm. Additionally, the linewidth of the laser must be narrower than that of the Hg^0 emission so that we can differentiate between the overlapping laser scatter and Hg^0 emission. An isotopically pure Hg-202 atomic resonance filter will be used to absorb spectrally narrow light resonant with the laser frequency, while transmitting a portion of the

*aahoops@sandia.gov; phone 1 925 294-3889; fax 1 925 294-2595

broader Hg^0 emission.[2] A laser linewidth ≤5 GHz (FWHM) is sufficient for this work. Performance modeling of the detection approach indicates that to meet the required sensitivity of ≤0.1 parts per billion (ppb) for the Hg^0 sensor, the average UV power for the laser must be ≥1 mW. For a high-repetition rate laser (10 kHz) that is compatible with photon-counting detection, this specification corresponds to a pulse energy of ≥0.1 μJ at 253.7 nm. Finally, the laser must have the requisite physical characteristics for use in a coal-fired power plant; the laser source should be compact, reliable, and have no consumables other than electricity.

Presently there are no commercial lasers that satisfy all of the aforementioned criteria. The laser architecture that we are pursuing to meet the needs of the Hg^0 sensor is a multistage nonlinear frequency-conversion design involving a fiber-amplifier-pumped optical parametric amplifier (OPA). Specifically, the OPA is pumped at 532 nm, and the seed source is a fiber-coupled, cw laser operating at 761.1 nm. The resultant signal beam is subsequently frequency tripled to yield 253.7-nm light. The current paper discusses performance modeling and component selection for the laser source (Section 2), construction of a breadboard frequency-converted OPA for testing (Section 3), and comparison of the measured performance to theoretical simulations (Section 4).

2. MODELING LASER PERFORMANCE

The laser for the Hg^0 sensor requires nonlinear crystals for (1) frequency doubling of 1064 nm, (2) optical parametric amplification of 761.1 nm, (3) frequency doubling of 761.1 nm, and (4) frequency mixing of 761.1 nm and 380.6 nm. Prior to assembly of the laser, we simulated the nonlinear mixing processes using SNLO,[3] a freely available software package developed at Sandia National Laboratories. SNLO calculates the expected output pulse energy, as well as spatial, temporal, and spectral profiles. The results of these calculations guided our selection of nonlinear crystals and focusing conditions. We chose the most practical crystals (i.e., highest damage threshold, non-hygroscopic) compatible with the required wavelengths and pulse energies.

2.1 Type I doubling of 1064 nm

The frequency-doubling conversion efficiency in a 10-mm long LBO crystal is calculated as a function of 1064-nm beam waist for several input beam energies that are attainable with a fiber amplifier,[4] and the results are presented in Fig. 1(a). We assume that the pulse duration of the perfectly Gaussian ($M^2 = 1$) 1064-nm beam is 1.0 ns (FWHM) and that the beam is focused in the center of the crystal. We conclude that a doubling efficiency of >60% is attainable for 1064-nm pulse energies ≥100 μJ. Furthermore, the resulting 532-nm beam is expected to have a nearly Gaussian profile, as shown by the calculated M^2 values presented in Fig. 1(b).

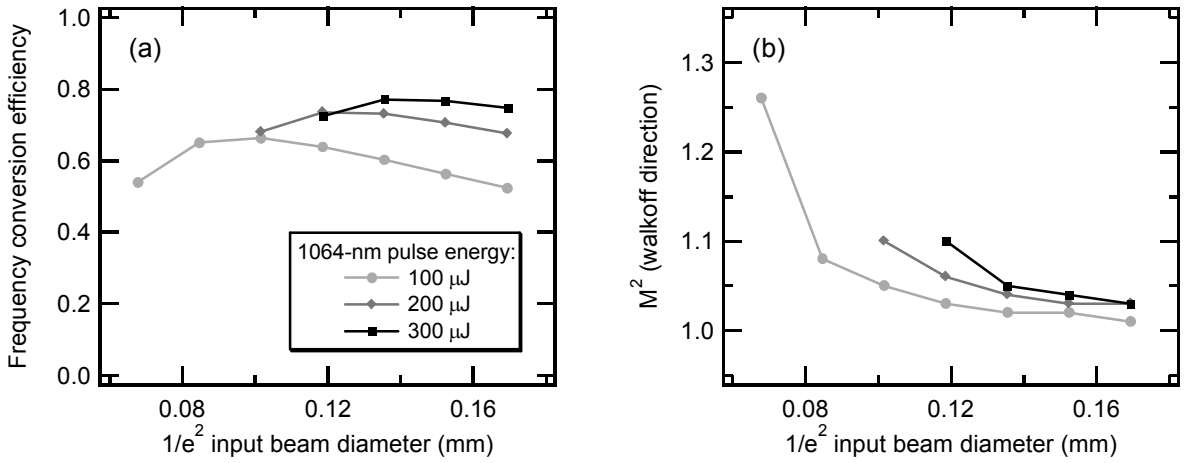

Fig. 1. Type I frequency doubling of 1064 nm in a 10-mm long LBO crystal for the input energies indicated: (a) conversion efficiency, and (b) M^2 values in the walkoff direction. The legend in (a) applies to both graphs.

2.2 Optical parametric amplifier

The 761.1-nm seed beam can be amplified in one of several periodically poled crystals. We consider MgO-doped $LiNbO_3$ and MgO-doped $LiTaO_3$. While periodically poled $LiNbO_3$ (PPLN) is more mature, periodically poled $LiTaO_3$ (PPLT) has a higher photorefractive-damage threshold and lower operating temperature. The amplified 761.1-nm pulse energies as a function of beam waist for several crystal lengths and pump energies are presented in Figs. 2(a, c) for PPLN and PPLT, respectively. As indicated in Fig. 1(a) and Ref. 4, 532-nm pulse energies ≥100 μJ are attainable, but we select 100 μJ as a conservative upper bound on the input pump energy. The seed power is 10 mW. The calculated M^2 values of the amplified signal beam as a function of output pulse energy are shown in Figs. 2(b, d), illustrating that lengthening the OPA crystal increases the M^2 value for equivalent 761.1-nm pulse energies. Moreover, in order to

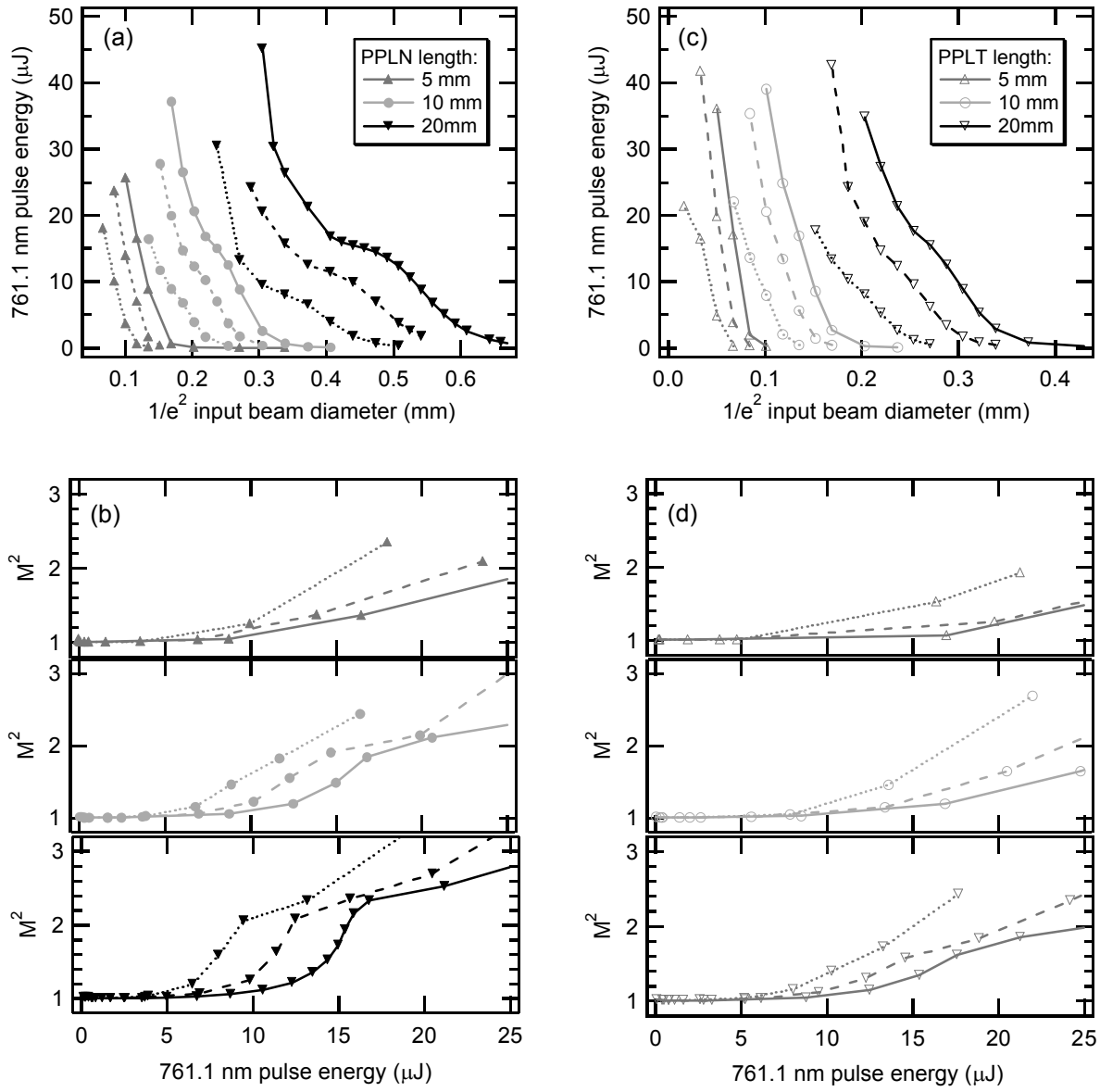

Fig. 2. Amplified 761.1 nm signal beam results for PPLN (a, b) and PPLT (c, d) for the crystal lengths indicated: (a, c) pulse energy, and (b, d) M^2 values. The legends in (a, c) also apply to (b, d). The solid, dashed, and dotted lines correspond to 532 nm pump energies of 100, 75, and 50 μJ, respectively.

maintain a constant amplified signal pulse energy, lowering the pump energy necessitates tighter focusing, which has a detrimental impact on the beam quality.

To ensure adequate beam quality for the subsequent nonlinear frequency-conversion steps, OPA crystals are chosen to provide 10 μJ of amplified signal pulse energy with a calculated $M^2 \leq 1.5$. Furthermore, PPLN and PPLT are available with maximum crystal heights of 0.5 mm and 1 mm, respectively. To pass 99% of the energy through the aperture defined by the crystal input face, the maximum $1/e^2$ beam diameters of the input beam are 0.32 mm and 0.64 mm for 0.5-mm and 1-mm tall crystals, respectively. For a pump pulse energy of 100 μJ and a seed laser power of 10 mW, our selection of crystal lengths narrows to 5 mm for PPLN, whereas PPLT lengths of 5, 10, or 20 mm are suitable. As indicated in Fig. 2(d), the shortest PPLT crystal length feasible should be selected for improved beam quality at a given amplified signal pulse energy. However, the tighter focusing conditions required for the 5-mm long PPLT and the associated risk for optical damage lead us to consider only the 10-mm long PPLT crystal. Our results indicate that the selected crystals will also be capable of yielding 10-μJ pulses at 761.1 nm with lower pump energies. The beam quality will be slightly degraded due to the need for tighter focusing but remains within the assumed specifications.

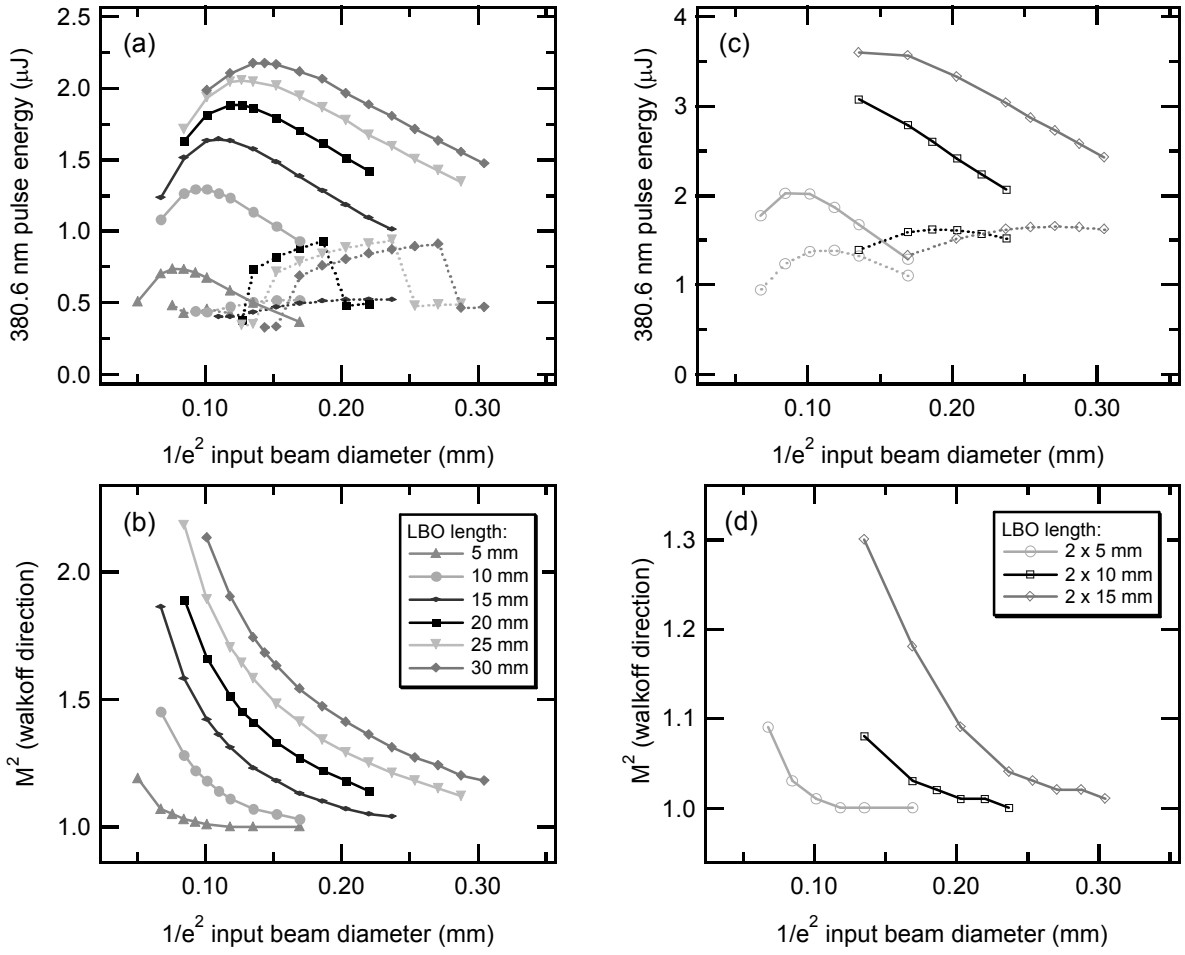

Fig. 3. Type I frequency doubling of 761.1 nm in LBO for a single crystal (a, b) and two crystals in a walkoff-compensating geometry (c, d) for the crystal lengths indicated: (a, c) 380.6-nm pulse energy for the entire beam (solid line) and Gaussian portion of the beam (dotted line), and (b, d) M^2 values in the walkoff direction. The legends in (b, d) also apply to (a, c).

2.3 Type I doubling of 761.1 nm

Frequency doubling of the amplified 761.1-nm signal beam in LBO is modeled with the assumption that the input pulse energy is 10 μJ. One focusing lens will be used for both of the nonlinear frequency-conversion steps following the OPA, providing a more compact design. We select the location of the beam focus to be 5 mm after the exit face of the LBO crystal. The resultant 380.6-nm pulse energies and M^2 values as a function of 761.1-nm beam waist for several LBO crystal lengths are presented in Figs. 3(a, b). The reduction in the spatial quality of the beam evident in Fig. 3(b) results from birefringent walkoff and will decrease the efficiency of the final frequency-conversion step. As a conservative estimate of this effect, we assume that only the portion of the 380.6-nm beam that has a Gaussian profile will contribute to the generation of 253.7-nm light. This approximation has been used successfully in past modeling of multistage frequency conversion.[5] The peak of the 380.6-nm beam is fit to a Gaussian in the direction perpendicular to the walkoff direction, and the resulting output pulse energies are included in Fig. 3(a).

As illustrated in Figs. 3(a, b), the beam quality can be improved by reducing the LBO crystal length, but at the cost of the frequency-doubling conversion efficiency. To maintain the high conversion efficiency of a longer crystal with the beam quality of a shorter crystal, two or more crystals can be used in a walkoff-compensating geometry.[6] Each crystal is rotated 180° about the beam path relative to the previous one. Thus, the spatial walkoff in one crystal is partially offset by the walkoff in the subsequent crystal, thereby improving the output beam quality and frequency-conversion

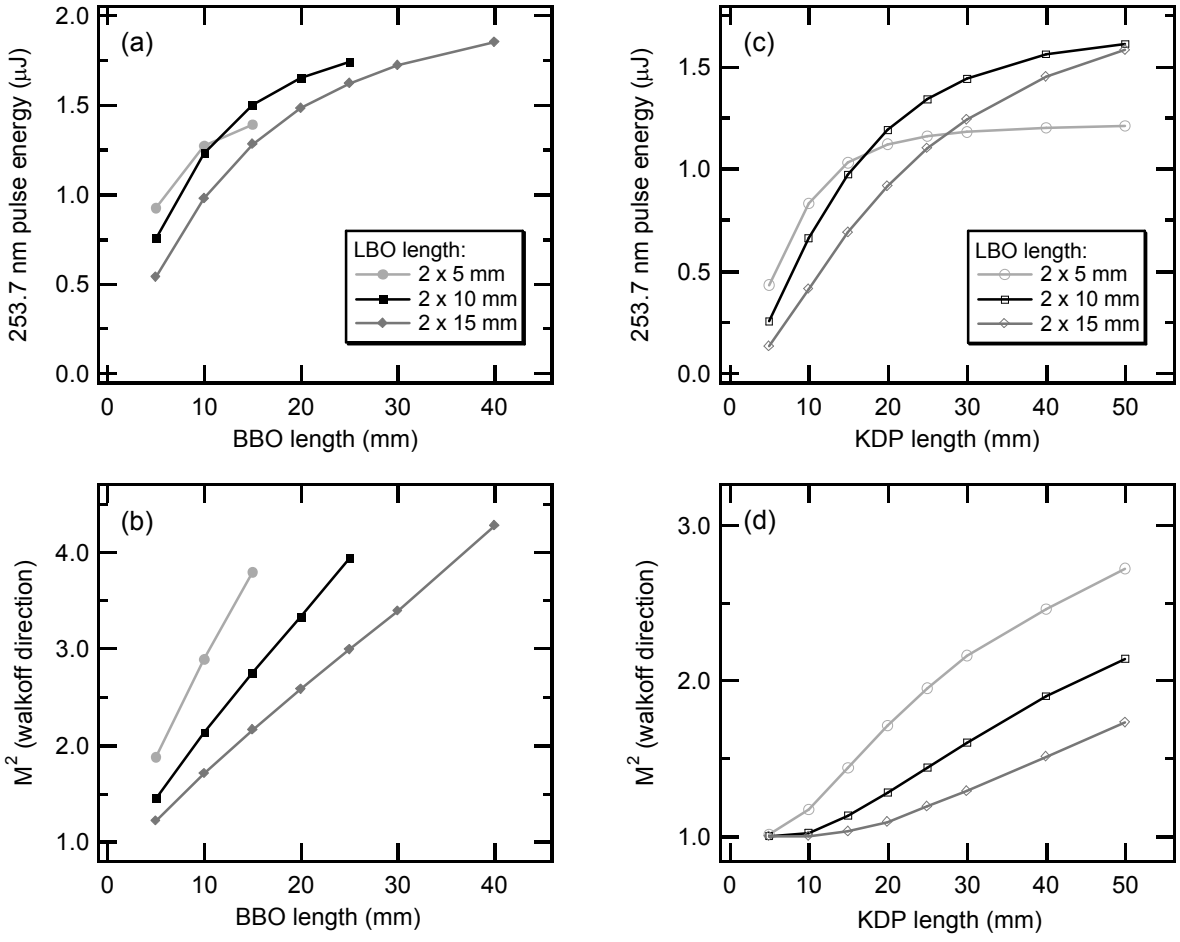

Fig. 4. Type I frequency mixing of 761.1 nm and 380.6 nm in BBO (a, b) and KDP (c, d) for the indicated LBO crystal lengths: (a, c) 253.7-nm pulse energy, and (b, d) M^2 values in the walkoff direction. The input beam parameters are obtained from the peak of the Gaussian portion of the 380.6-nm beam generated by the previous frequency-conversion step. The legends in (a, c) also apply to (b, d).

efficiency. In this orientation, the frequency-doubling conversion efficiency is determined by the sum of the crystal lengths. The calculated pulse energies for the entire beam and Gaussian portion for several crystal lengths in a two-crystal, walkoff-compensating geometry are shown in Fig. 3(c). Additionally, the M^2 values are presented in Fig. 3(d), highlighting the improved beam quality in comparison to a single LBO crystal. For the laser design, we select the walkoff-compensating geometry with two 10-mm LBO crystals as the optimum balance of output pulse energy and beam quality.

2.4 Type I mixing of 761.1 nm and 380.6 nm

The 761.1-nm and 380.6-nm beams output by the LBO crystals can be frequency mixed in either BBO or KDP to generate 253.7-nm light. Using the 761.1-nm beam waists that maximize the pulse energies of the Gaussian portion of the 380.6-nm beam, we model the final nonlinear frequency-conversion process for several lengths of BBO and KDP. The input beam is assumed to be focused 5 mm in front of the entrance face of the final nonlinear crystal. The 253.7-nm pulse energies and M^2 values determined for BBO and KDP are shown in Fig 4. Although the maximum 253.7-nm pulse energy is slightly higher for BBO, the output beam quality for KDP is superior. In contrast to the other wavelengths generated, the 253.7-nm beam has no beam quality requirements for subsequent frequency conversion. However, lower M^2 values will allow tighter focusing of the 253.7-nm beam, thereby enabling the use of a narrower detector field-of-view to reduce the collection of laser scatter. As a compromise between maximum output pulse energy at 253.7 nm and beam quality, we select a 50-mm long KDP crystal, which is expected to generate 1.6-μJ pulses. Given that the required 253.7-nm pulse energy is 0.1 μJ, our design offers substantial engineering margin.

3. EXPERIMENTAL

The modeling results discussed in Section 2 guide our selection of the appropriate components for the OPA and frequency doubling and tripling stages. The ultimate 532-nm pump source, a frequency-doubled pulsed fiber amplifier, is currently under development. Nevertheless, we can assess the performance of the OPA and subsequent frequency-conversion stages using another 532-nm source, the frequency-doubled output of a passively Q-switched, monolithic Nd:YAG microlaser.[7] This laser is pulse-pumped by a 45-W fiber-coupled diode laser (Jenoptik, JOLD-45-CPXF-1L) at a 10-Hz repetition rate. We operate the microlaser at a 10-Hz repetition rate and with temperature stabilization to ensure single-longitudinal-mode operation. Although the microlaser is operating at a lower repetition rate than that desired for the Hg^0 sensor, the output pulse energy is comparable to that expected from the fiber amplifier. Thus, we can characterize and optimize the nonlinear frequency-conversion stages.

With the exception of the fiber-coupled lasers, the entire light source is mounted on a 45.7 cm × 30.5 cm breadboard and is depicted schematically in Fig. 5. A half-wave plate in combination with a linear polarizer is included in the design to

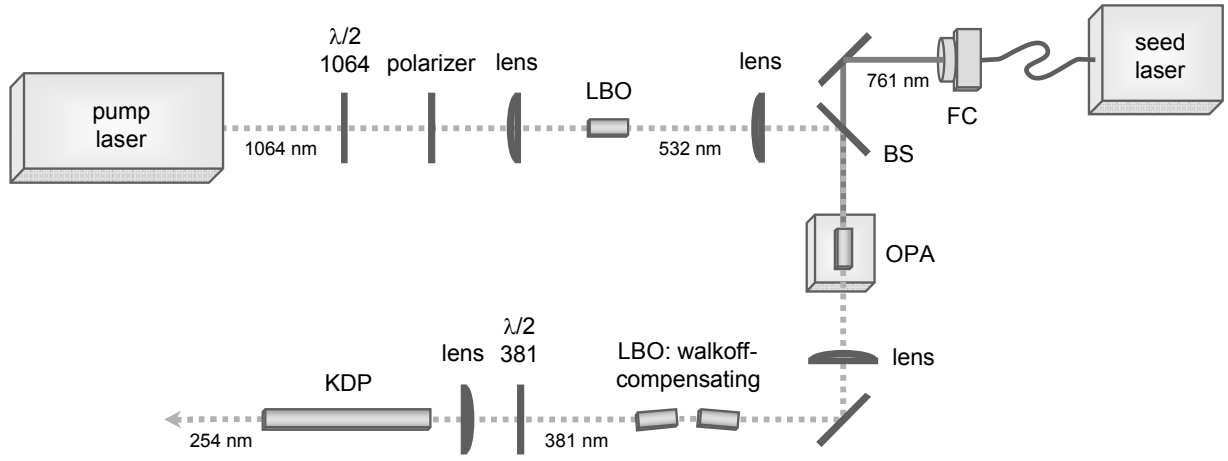

Fig. 5. Diagram of laser for Hg^0 sensor. FC, fiber coupler; λ/2, half-wave plate at the designated wavelength in nm; BS, beam splitter. Straight dashed and solid lines denote free-space pulsed and cw beams, respectively. The curved line represents a fiber.

allow adjustment of the 1064-nm pulse energy. The 1064-nm beam is frequency doubled in LBO (Castech, 10-mm long, XY cut, $\theta = 90°, \phi = 12°$) using Type I phase matching. The resulting 532-nm beam is used to pump the OPA. The OPA employs a MgO-doped PPLT crystal (HC Photonics Corp., 10-mm long, period: 9.11 μm) temperature stabilized to ~40°C. The temperature of the oven can be adjusted to tune the wavelength of the output signal beam, and the temperature controller stabilizes the bulk oven temperature to 0.1°C. The OPA is seeded by a fiber-coupled, tunable, cw distributed-feedback diode laser (Sacher Lasertechnik Group, SYS 050-DFB-0760.98-40) tuned to 761 nm. The seed laser has a total tuning range of 2 nm and maximum output power of 9 mW. The amplified 761-nm signal beam is Type I frequency doubled in two LBO crystals (Castech, 10-mm long, XY cut, $\theta = 90°$, $\phi = 36.5°$) in a walkoff-compensating geometry. Finally, 254-nm light is generated by Type I mixing of the 761-nm and 381-nm beams in KDP (Castech, 50-mm long, 76.5°). A zero-order waveplate (full-wave at 761 nm, half-wave at 381 nm) is placed between the walkoff-compensating LBO crystals and the KDP crystal to rotate the polarization of the 381-nm beam to be parallel to that of the 761-nm beam. The nonlinear crystals are positioned near the beam waists provided by the lenses and are angle tuned to maximize the 254-nm pulse energy. Note that, compared to the calculations described in the previous section, an additional lens is inserted before the KDP crystal to ensure proper focusing of the beams for the final nonlinear frequency-conversion stage. The frequency-conversion efficiencies, spectral properties, and spatial profiles of the laser are characterized using pyroelectric energy meters, an optical spectrum analyzer (OSA), an etalon with a 5.16-GHz free spectral range, and a CCD camera.

4. RESULTS AND DISCUSSION

4.1 Type I doubling of 1064 nm

In Section 2, we assumed that the 1064-nm input beam had a 1.0-ns FWHM temporal width and was perfectly Gaussian. The actual 1064-nm pulse of the microlaser has a duration of 2.0 ns (FWHM) with a measured M^2 of 1.4, and the beam is focused to a $1/e^2$ waist diameter of 0.10 mm. Using these measured pulse parameters, we recalculate the expected 532-nm pulse energy with SNLO, and the measured frequency-doubling conversion efficiency is in excellent agreement with the calculations (Fig. 6). At the maximum 1064-nm input energy of 200 μJ, the measured conversion efficiency is 69%.

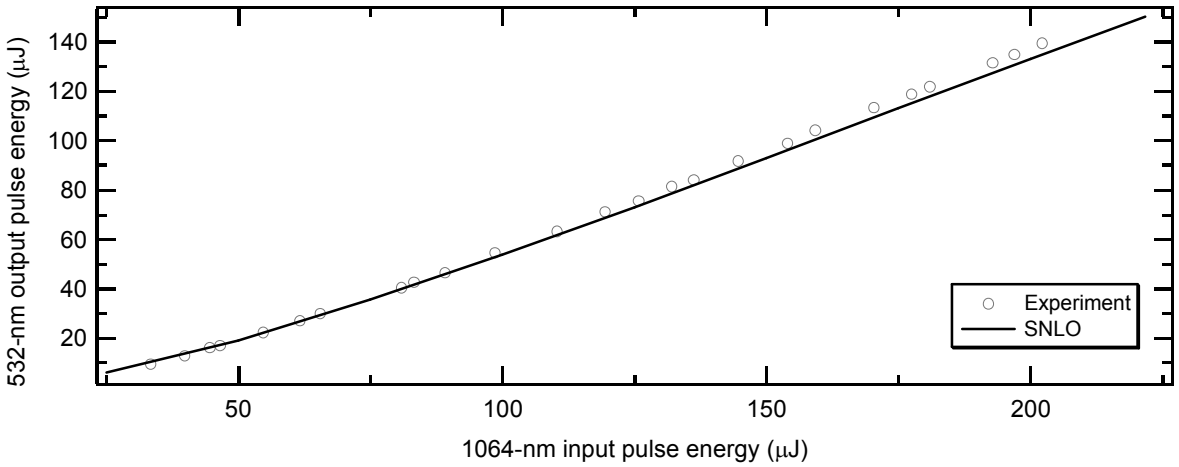

Fig. 6. Frequency-doubling conversion efficiency of 1064 nm in LBO. The symbols are the experimentally measured output pulse energies, and the solid line is that predicted by SNLO.

4.2 Optical parametric amplifier

The performance of the OPA is evaluated by two methods. First, we compare the unseeded 761-nm signal beam spectrum to that generated with the addition of the seed laser. Unseeded, the PPLT operates as an optical parametric generator, with the unseeded output signal beam spanning 0.5 nm (FWHM) as measured using the OSA. Upon seeding, the amplified signal beam spectrally narrows to less than the 0.015-nm resolution limit of the OSA, and the out-of-band

signal is suppressed by 23 dB. The ratio of the in-band to out-of-band pulse energy for the OPA is 28 dB. Second, the linewidths of the seed laser and amplified 761-nm signal beam are measured using the etalon and CCD camera. The measured seed laser linewidth is <230 MHz (FWHM), limited by the instrument resolution. The linewidth (FWHM) of the amplified signal beam is 723 ± 42 MHz.

We observe that the wavelength of the amplified signal beam is not solely determined by the seed laser wavelength. By adjusting the oven temperature of the OPA, we can affect not only the ability of the 761-nm beam to seed the OPA, but also the wavelength of the amplified signal beam. This effect occurs because the peak gain wavelength is determined by the poling period, which is sensitive to temperature. The temperature dependence is illustrated by the change in spectral

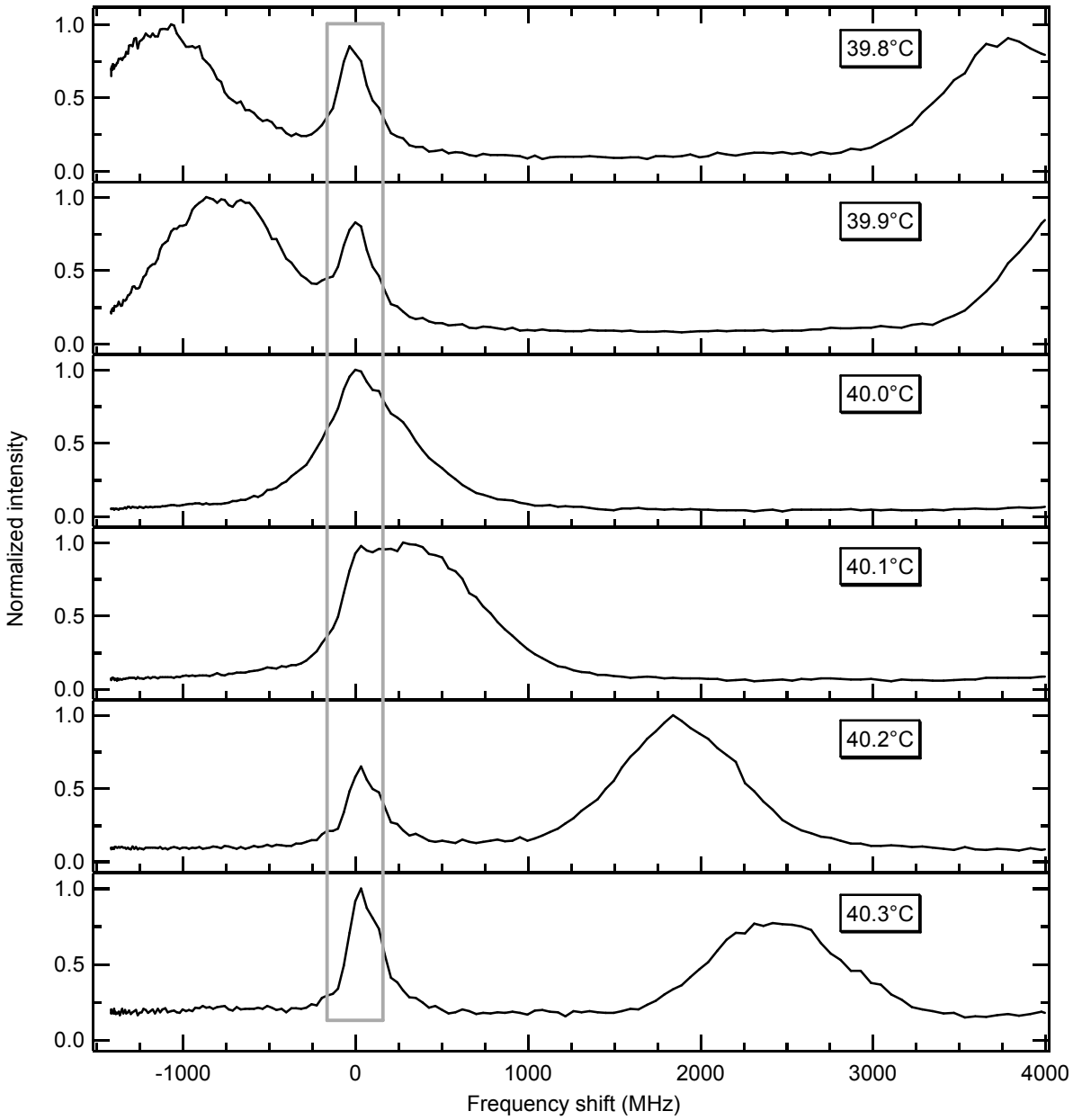

Fig. 7. Shift in amplified signal beam frequency with OPA oven temperature. The black curves are radial slices of the etalon fringes for the oven temperatures indicated, and the grey rectangle denotes the position of the etalon fringe of the seed laser.

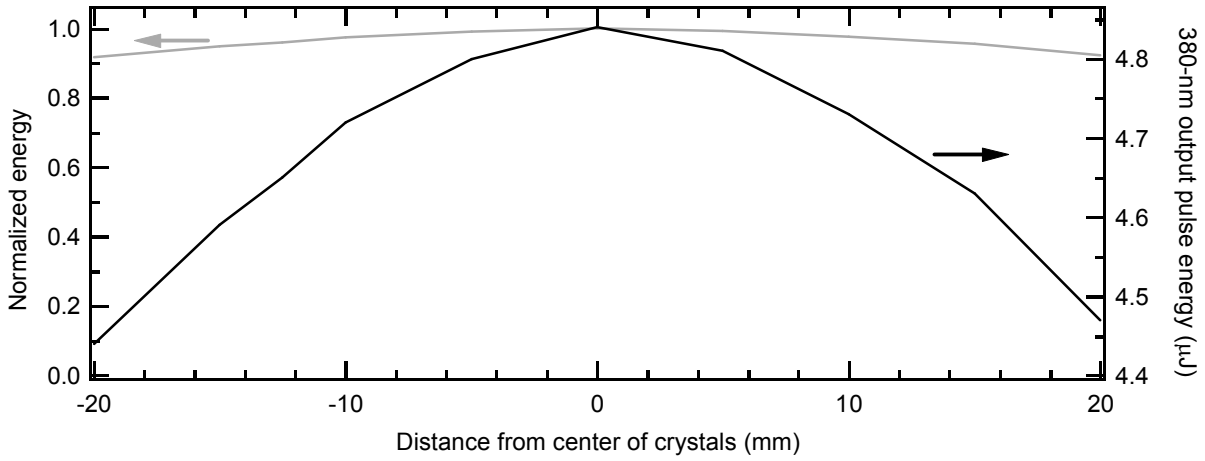

Fig. 8. SNLO calculations of frequency-doubling conversion efficiency of 761-nm beam as a function of beam focus location. The input pulse energy is 14 μJ, and the $1/e^2$ beam waist diameter is 0.19 mm. The normalized and absolute output pulse energies are plotted on the left and right axes, respectively.

overlap between the seed laser and amplified signal beam presented in Fig. 7. The OPA can be well-seeded at wavelengths offset up to 2.5 GHz from the seed laser wavelength. A consequence of this phenomenon is that the amplified signal wavelength cannot be assumed to be equal to the seed laser wavelength. In addition, temperature stabilization better than 0.1°C is required for good output wavelength stability.

4.3 Type I doubling of 761 nm

The amplified signal beam from the OPA is focused to a $1/e^2$ waist diameter of 0.19 mm within 1 mm of the input face of the first walkoff-compensating LBO crystal. Space constraints on the optical breadboard preclude mounting the focusing lens on a translational stage to optimize the location of the beam waist. Although focusing the beam in the center of the crystals is preferred, SNLO calculations indicate that varying the location of the beam waist over the length of the crystals only lowers the output pulse energy by a few percent (Fig. 8). The frequency-doubling conversion efficiency for this stage is presented in Fig. 9 along with that predicted by SNLO. The calculations and experimental results are in close agreement. A conversion efficiency of 31% is measured at the maximum 761-nm input energy of 14 μJ.

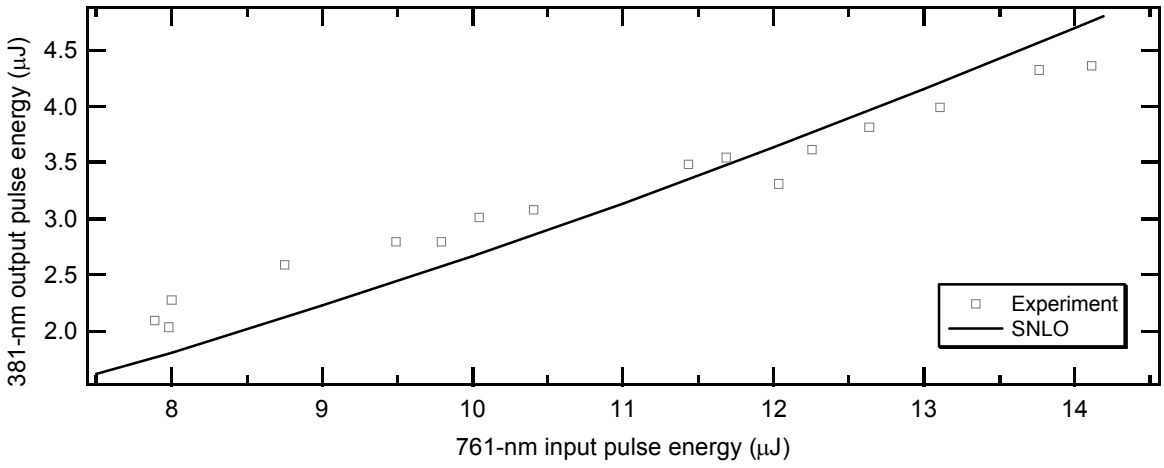

Fig. 9. Frequency-doubling conversion efficiency of 761 nm in two LBO crystals in a walkoff-compensating geometry. The symbols are the experimentally measured output pulse energies, and the solid line is that predicted by SNLO.

4.4 Type I mixing of 761 nm and 381 nm

In the final nonlinear frequency-conversion step, the 761-nm and 381-nm beams are focused into the KDP crystal with a $1/e^2$ beam waist diameter of 0.13 mm. The frequency-conversion efficiency for this final stage is 63% below that predicted by SNLO for perfect beam overlap. This disparity results from poor overlap between the 761-nm and 381-nm beams, which could be significantly improved in an optimized setup. However, for the maximum input energies measured, 13 μJ and 6.0 μJ of 761-nm and 381-nm light, respectively, the 254-nm output beam has a pulse energy of 1.8 μJ. Note that our analysis indicated that the required pulse energy is 0.1 μJ. Given that the 254-nm pulse energy is 18× that required and the need for laser compactness, we elected not to use additional optics to improve the spatial overlap of the 761-nm and 381-nm beams.

5. CONCLUSIONS

We have designed and evaluated the performance of a 254-nm laser source suitable for detecting Hg^0 emissions from coal-fired power plants. The measured output pulse energy of the laser is 1.8 μJ, well exceeding the desired 0.1-μJ pulse energy. Ongoing efforts in our laboratory are directed towards characterizing the linewidths of the 381-nm and 254-nm beams. In addition, the Nd:YAG microlaser will be replaced with a microchip-seeded fiber amplifier operating at a repetition rate >10 kHz.[4] The higher repetition rate of this pump source is compatible with photon-counting detection and will yield significantly higher average power for the UV laser, thereby enabling sub-ppb detection limits for Hg^0 emissions. More generally, the frequency-converted OPA presented in this work provides a compact, all-solid-state source of tunable, narrow-linewidth visible and ultraviolet radiation, which is required for many chemical sensing applications.

This work is supported by the DOE Office of Fossil Energy's National Energy Technology Laboratory Advanced Research Program through DOE award FEW03-011948. Sandia is a multiprogram laboratory operated by Sandia Corporation, a Lockheed Martin Company, for the United States Department of Energy's National Nuclear Security Administration under contract DE-AC04-94AL85000.

REFERENCES

[1] A. A. Hoops, T. A. Reichardt, D. A. V. Kliner, J. P. Koplow, and S. W. Moore, "Detection of mercuric chloride by photofragment emission using a frequency-converted fiber amplifier," Appl. Opt. **46**, 4008-4014 (2007).

[2] A. P. Yalin and R. B. Miles, "Temperature measurements by ultraviolet filtered Rayleigh scattering using a mercury filter," J. Thermophys. Heat Transfer **14**, 210-215 (2000).

[3] SNLO nonlinear optics code available from A. V. Smith, Sandia National Laboratories, Albuquerque, NM 87185-1423.

[4] P. E. Schrader, R. L. Farrow, D. A. V. Kliner, J. -P. Fève, and N. Landru, "High-power fiber amplifier with widely tunable repetition rate, fixed pulse duration, and multiple output wavelengths," Opt. Express **14**, 11528-11538 (2006); P. E. Schrader, R. L. Farrow, D. A. V. Kliner, J. -P. Fève, and N. Landru, "Fiber-based laser with tunable repetition rate, fixed pulse duration, and multiple wavelength output," Proc. of SPIE Vol 6453, 64530D (2007).

[5] D. A. V. Kliner, F. Di Teodoro, J. P. Koplow, S. W. Moore, and A. V. Smith, "Efficient second, third, fourth, and fifth harmonic generation of a Yb-doped fiber amplifier," Opt. Commun. **210**, 393-398 (2002).

[6] A. V. Smith, D. J. Armstrong, W. J. Alford, "Increased acceptance bandwidths in optical frequency conversion by use of multiple walk-off-compensating nonlinear crystals," J. Opt. Soc. Am. B **15**, 122-141 (1998).

[7] K. W. Aniolek, R. L. Schmitt, T. J. Kulp, B. A. Richman, S. E. Bisson, and P. E. Powers, "Microlaser-pumped periodically poled lithium niobate optical parametric generator-optical parametric amplifier," Opt. Lett. **25**, 557-559 (2000).